CHEMISTRY

A polyaromatic nanocapsule as a sucrose receptor in water

Masahiro Yamashina,[1]* Munetaka Akita,[1] Taisuke Hasegawa,[2†] Shigehiko Hayashi,[2] Michito Yoshizawa[1‡]

Selective recognition of saccharides by artificial receptors in water is a challenging goal due to their strong hydrophilicities and complex molecular structures with subtle regio- and stereochemical differences. We report the selective and efficient encapsulation of D-sucrose within a coordination-driven molecular capsule from natural saccharide mixtures in water (~100% selectivity, >85% yield, and ~10^3 M^{-1} binding constant). Unlike previous artificial receptors and natural receptors that rely on multiple hydrogen-bonding interactions, theoretical calculations and control experiments indicate that the observed unique selectivity arises from multiple CH-π interactions between the sucrose hydrocarbon backbone and the shape-complementary polyaromatic cavity (~1 nm in diameter) of the capsule.

INTRODUCTION

Hydrogen bonds are a ubiquitous and indispensable tool in the selective binding of guest substrates by enzymes and biological receptors (*1*). Even in water, where hydrophilic natural compounds such as saccharides are fully solvated by water molecules through extensive hydrogen bonds (*1*–*3*), the protein surfaces and active sites precisely discriminate subtle stereo- and regiochemical differences in the complex structures (Fig. 1A) (*4*–*6*). The Davis group demonstrated that isophthalamide-based organic cages can efficiently accommodate monosaccharides such as D-glucose (binding constant: K_a = up to 190 M^{-1}) (*7*) and disaccharides such as D-cellobiose (K_a = up to 3300 M^{-1}) (*8*, *9*) in water through hydrogen bonds and CH-π interactions. Similar cooperative interactions (*10*), reversible covalent bonds (*11*), coordinative interactions (*12*), and ion-dipole interactions (*13*) were also used for the recognition of natural saccharides in water. However, strict discrimination of saccharides in water remains an extremely hard task for synthetic molecular receptors (*14*–*16*). To further develop artificial receptors as novel sensing devices (*17*) and to provide mechanistic insights into biological recognition events such as taste (*18*–*20*), here we demonstrate a new recognition motif using a molecular cavity enclosed by polyaromatic frameworks (Fig. 1B) that exclusively bind D-sucrose in water. D-Sucrose is one of the most common natural compounds in our daily life, yet the relatively large and bulky structure (a ~1 nm length and ~300 $Å^3$ volume) prevents it from full encapsulation by traditional covalent hosts (*7*–*16*). On the other hand, coordination-driven molecular cages and capsules (*21*–*25*) are available in a much larger range of cavity sizes and shapes, suitable for large guest substrates. However, because of the lack of effective bonding motifs, the recognition and binding of saccharides within coordination host compounds remain very rare, even in organic media (*26*, *27*).

The encapsulation of polyaromatic fullerene guests by saccharide-based molecular hosts, that is, cyclodextrin dimers, in water has been reported by several groups (*28*–*30*). The intriguing host-guest complexes prompted us to invert the relationship and use a polyaromatic-shelled host (*31*, *32*) for the selective recognition of saccharide guests. We used coordination-driven molecular capsule **1**, which has a spherical cavity (~1 nm in diameter and ~580 $Å^3$ in volume) surrounded by polyaromatic anthracene panels (Fig. 1, C and D) (*33*). Although the host capability of **1** toward various hydrophobic compounds (for example, adamantanes, pyrenes, and fullerene C_{60}) is well known (*33*–*36*), the potential for binding

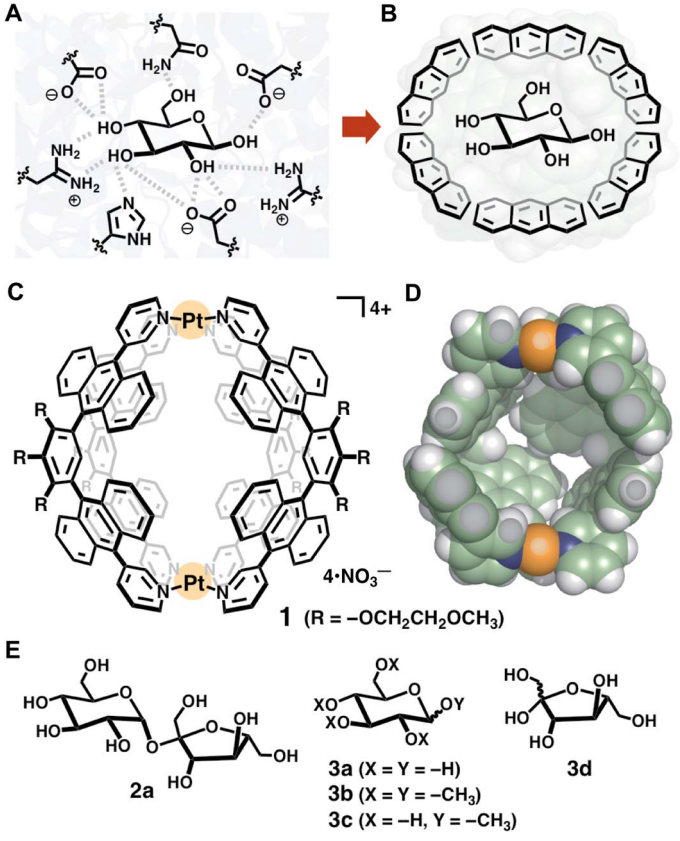

Fig. 1. Cartoon representation of saccharide recognitions and structures of a polyaromatic nanocapsule and saccharides. Recognition of D-glucose (**A**) in a hydrogen-bonding cavity modeled after the binding site of sucrose hydrolase (E322Q-glucose complex) from *Xanthomonas axonopodis* pv. glycines (*6*) and (**B**) in a polyaromatic cavity. (**C**) Coordination-driven polyaromatic nanocapsule **1** and (**D**) its slice through the center of the crystal structure [space-filling model; substituents (R) are replaced by hydrogen atoms for clarity]. (**E**) D-Sucrose (**2a**), glucose derivatives **3a** to **3c**, and D-fructose (**3d**) used as guest molecules.

[1]Laboratory for Chemistry and Life Science, Institute of Innovative Research, Tokyo Institute of Technology, 4259 Nagatsuta, Midori-ku, Yokohama 226-8503, Japan.
[2]Department of Chemistry, Graduate School of Science, Kyoto University, Kitashirakawa, Oiwakecho, Sakyo, Kyoto 606-8502, Japan.
*Present address: Department of Chemistry, University of Cambridge, Lensfield Road, Cambridge CB2 1EW, UK.
†Present address: Molecular Spectroscopy Division, Max-Planck-Institut für Polymerforschung, Ackermannweg 10, 55128 Mainz, Germany.
‡Corresponding author. Email: yoshizawa.m.ac@m.titech.ac.jp

highly hydrophilic biomolecules in the hydrophobic cavity of **1** was rather unexpected. Nevertheless, we report here that nanocapsule **1** can effectively encapsulate D-sucrose (**2a**; $K_a \geq 1100\ M^{-1}$) from mixtures of **2a** and other natural disaccharides in water with perfect selectivity. Theoretical host-guest calculations and control binding experiments with D-glucose derivatives **3a** to **3c** (Fig. 1E) indicate that the observed unique selectivity stems from multiple CH-π interactions between the hydrocarbon framework of **2a** and the shape-complementary polyaromatic cavity of **1**.

RESULTS

Encapsulation of monosaccharides

We initially examined host-guest interactions between nanocapsule **1** and natural monosaccharides, such as D-glucose (**3a**), D-fructose (**3d**), and D-mannose, in water. For example, when a mixture of **1** (0.39 μmol) and slight excess **3a** (2.0 μmol) was stirred in D_2O (0.5 ml) at 60°C for 30 min (scheme S1), neither new peaks nor peak shifts (expected for host-guest interactions) were observed in the proton nuclear magnetic resonance (^{1}H NMR) and electrospray ionization–time-of-flight (ESI-TOF) mass spectrometry (MS) spectra of the resultant solution (Fig. 2, A and B). No interactions were also observed for the other monosaccharides (figs. S1 and S2). These results are explicable by usual hydrophilic and hydrophobic properties: The highly hydrophilic saccharides preferentially exist in the aqueous phase rather than the hydrophobic cavity of **1**.

In contrast, one molecule of pentamethylated α-D-glucose **3b** was quantitatively encapsulated within capsule **1** under the same conditions (Fig. 2A, right, and scheme S2) (*37*), although **3b** is very soluble in water (>50 mM). The 1:1 host-guest complex **1**⊃**3b** exhibited ^{1}H NMR signals derived from the methyl groups of encapsulated **3b** ranging from −0.45 to 1.03 parts per million (ppm) (Fig. 2C, left, and figs. S3 and S4). These signals are significantly shifted upfield ($\Delta\delta_{max}$ = −3.86 ppm), compared with free **3b** in D_2O, because of the shielding effects of the nearby anthracene rings. Close contact between

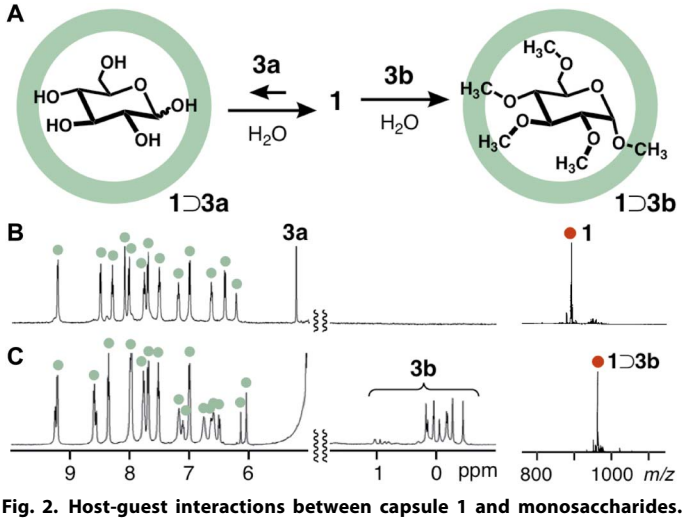

Fig. 2. Host-guest interactions between capsule 1 and monosaccharides. (**A**) Schematic representation of host-guest interactions between capsule **1** and D-glucose (**3a**) or pentamethylated α-D-glucose **3b** in H_2O. ^{1}H NMR spectra (500 MHz, D_2O, room temperature; left) and ESI-TOF MS spectra (H_2O, room temperature, tetravalent molecular ion peak; right) of (**B**) a mixture of **1** and **3a**, and (**C**) host-guest complex **1**⊃**3b**.

1 (protons $H_{f,b'}$) and **3b** (CH_3 groups) in the cavity was confirmed by one-dimensional (1D) nuclear Overhauser effect spectroscopy (NOESY) NMR studies (fig. S5). The noncovalent host-guest **1**⊃**3b** complex is highly stable in water; we estimated the binding constant at $>10^8\ M^{-1}$ from ^{1}H NMR and MS analyses under high-dilution conditions (5.0 μM; figs. S6 and S7) (*37*). The ESI-TOF MS spectrum only displayed prominent peaks from the intact host-guest structure [for example, mass-to-charge ratios (*m/z*) of 1995.4 for $[\mathbf{1}\supset\mathbf{3b} - 2\bullet NO_3^-]^{2+}$, 1309.6 for $[\mathbf{1}\supset\mathbf{3b} - 3\bullet NO_3^-]^{3+}$, and 966.7 for $[\mathbf{1}\supset\mathbf{3b} - 4\bullet NO_3^-]^{4+}$; Fig. 2C, right, and fig. S8]. The optimized structure of **1**⊃**3b** indicates that the four CH_3 groups of **3b** are in close proximity (~3.6 Å) to the anthracene panels of **1** (fig. S9). The strong host-guest interactions observed between **1** and **3b** are mainly caused by hydrophobic CH-π (polyaromatic) interactions in the confined cavity (*38*–*41*). Monomethylated α-D-glucose **3c** was also bound by capsule **1** in 81% yield (figs. S1C and S2C). These unusual binding affinities prompted us to further examine host-guest interactions between the polyaromatic capsule and natural disaccharides.

Encapsulation of disaccharides

We next investigated aqueous binding for common disaccharides, D-sucrose, D-lactose, D-maltose, and D-trehalose (scheme S3), and thereby, efficient encapsulation by capsule **1** was observed for only D-sucrose (**2a**). Upon mixing **1** (0.39 μmol) with **2a** (2.0 μmol) in D_2O (0.5 ml) for 30 min at 60°C, 1:1 host-guest complex **1**⊃**2a** was formed in 86% yield (Fig. 3A, right, and figs. S10 and S11). In the ^{1}H NMR spectrum, all signals for the host and guest were assigned by 2D NMR studies (Fig. 3B and figs. S12 to S15). The methine signals $H_{A-E,G-I}$ and methylene signals $H_{F,J,K}$ of encapsulated **2a** were found in the range of −1.14 to 1.29 ppm due to aromatic shielding ($\Delta\delta_{max}$ = −4.64 ppm). Broadening of the anthracene signals H_{c-e} of **1** (at 6.5 to 7.2 ppm) suggests restricted motion of the polyaromatic panels upon encapsulation of the relatively large guest **2a**. The number of the host proton signals of **1**⊃**2a** is the same as that of empty **1**, indicating full inclusion of **2a** in the capsule cavity. The ^{1}H diffusion-ordered spectroscopy (DOSY) NMR spectrum revealed the presence of a single host-guest species (Fig. 3C and fig. S16). A 1:1 host-guest composition was unambiguously confirmed by the ESI-TOF MS analysis, which showed prominent peaks at *m/z* values of 2041.7, 1340.5, and 989.9 assignable to $[\mathbf{1}\supset\mathbf{2a} - n\bullet NO_3^-]^{n+}$ species (n = 2, 3, and 4, respectively; Fig. 3E and fig. S17). Host-guest interactions were undetected for **1** and the other disaccharides in water (fig. S18). Furthermore, the formation of the ternary complex **1**⊃(**3a**•**3d**) was not observed upon combination of **1** and an equimolar mixture of **3a** and D-fructose (**3d**) (5 eq each), which are components of **2a**, even under various conditions (Fig. 3A, left, and D).

To elucidate detailed host-guest interactions, we estimated theoretical binding free energies of **1**⊃**2a** and the related host-guest complexes in water by comparing the solvation free energies of the saccharide guests and intermolecular host-guest interactions (*42*). The binding energy of **1**⊃**2a** is lower than that of host-guest complexes such as **1**⊃(D-trehalose) and **1**⊃(D-lactose) (−10.2 and −37.2 kcal mol^{-1}, respectively) and higher than that of **1**⊃**3b** (11.0 kcal mol^{-1}) (table S1). These results are consistent with the ^{1}H NMR–binding experiments. In the optimized structure (Fig. 3F and figs. S19 and S20), encapsulated **2a** adopts a spherical conformation in the spherical cavity of **1**. The conformation is supported by the NOESY NMR analysis, where correlation signals are observed between the pyranose and furanose moieties (H_E–H_J and H_A–H_K) of **2a** (fig. S13). The three CH_2 groups of **2a** are in close contact (<3.8 Å) with the polyaromatic panels of **1** in the optimized

structure (Fig. 3F). Thermodynamic parameters for the host-guest interactions of **1**⊃**2a** in water were determined by a van't Hoff plot (Fig. 3G) using temperature-dependent ^{1}H NMR analysis (fig. S21 and table S2). The obtained positive value of entropy (8.00 cal mol^{-1} K^{-1}) and negative value of enthalpy (−1.90 kcal mol^{-1}) indicate that the encapsulation process is driven mainly by enthalpic stabilization. The binding constant was also calculated to be 1170 ± 120 M^{-1} at 25°C (fig. S22 and table S3).

Selective recognition of D-sucrose

Nanocapsule **1** is a working sucrose receptor and selectively binds D-sucrose even from mixtures of natural disaccharides in water. To illustrate this instance, the **1**⊃**2a** complex exclusively formed from a D_2O solution containing **1** and a mixture of **2a** and D-trehalose (**2b**) (5 eq each) for 30 min at 60°C (Fig. 4A). The upfield region ^{1}H NMR spectrum of the resultant solution displayed only peaks when corresponding to encapsulated **2a** (Fig. 4, B and C). The host-guest complex could be isolated as a pale yellow solid (in 80% yield; Fig. 4D and fig. S23) from the aqueous solution by salting out with a grain of KNO_3. The sucrose-bound capsule **1**⊃**2a** was selectively obtained from all competitive binding experiments with **2a** and other disaccharides [that is, D-lactose (**2c**), D-maltose (**2d**), D-cellobiose (**2e**), and D-lactulose (**2f**); Fig. 4, E and F], as revealed by ^{1}H NMR analysis (fig. S24). On the basis of the present experimental and theoretical studies, we postulate that the observed strict discrimination stems from an effective steric match and multiple CH-π interactions between the

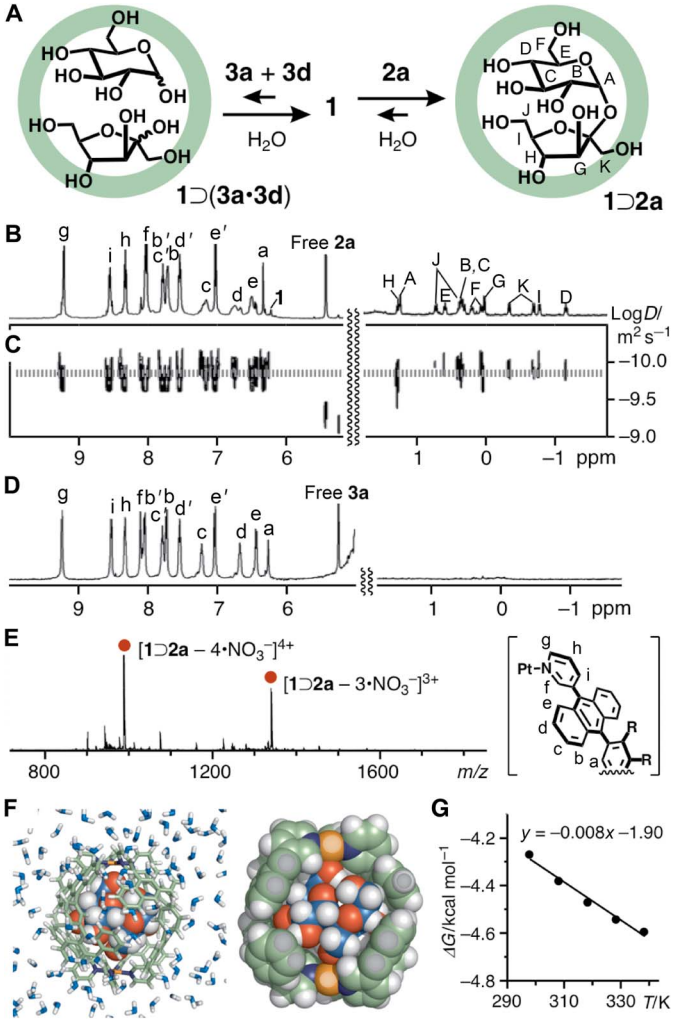

Fig. 3. Encapsulation of D-sucrose within capsule 1 in water. (**A**) Schematic representation of host-guest interactions between capsule **1**, D-glucose (**3a**), and D-fructose (**3d**) (left) and the encapsulation of D-sucrose (**2a**) within **1** (right). (**B**) ^{1}H NMR and (**C**) ^{1}H DOSY NMR spectra (500 MHz, D_2O, room temperature) of **1**⊃**2a**. (**D**) ^{1}H NMR spectrum (500 MHz, D_2O, room temperature) of a mixture of **3a** and **3d** with **1**. (**E**) ESI-TOF MS spectrum (H_2O, room temperature) of **1**⊃**2a**. (**F**) Structure of **1**⊃**2a** in water (left) and its slice through the center (right) (substituents and counterions are omitted for clarity). (**G**) van't Hoff plot for the thermodynamic parameters of **1**⊃**2a**.

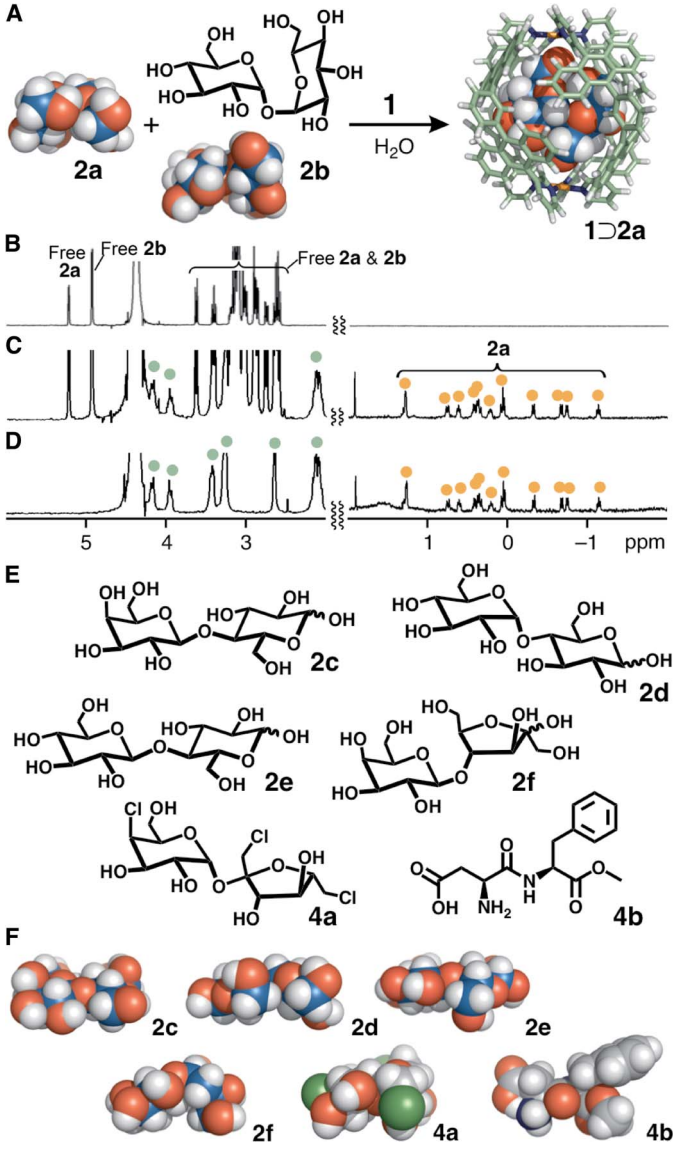

Fig. 4. Selective recognition of D-sucrose and structures of disaccharides and artificial sugars. (**A**) Schematic representation of the selective encapsulation of D-sucrose (**2a**) from a mixture of **2a** and D-trehalose (**2b**) by capsule **1**. ^{1}H NMR spectra (500 MHz, D_2O, room temperature) of (**B**) **2a** and **2b**, (**C**) a mixture of **1**⊃**2a**, **2a**, and **2b**, and (**D**) isolated **1**⊃**2a**. (**E**) D-Lactose (**2c**), D-maltose (**2d**), D-cellobiose (**2e**), D-lactulose (**2f**), sucralose (**4a**), and aspartame (**4b**) used as guest molecules and (**F**) their optimized structures [density functional theory (DFT), B3LYP/6-31G(d); conductor-like polarizable continuum model (CPCM; H_2O) level].

hydrocarbon backbone of sucrose and the polyaromatic interior surface of capsule **1**.

Note that the artificial cavity of capsule **1** could quantitatively and strongly bind artificial sugar substitutes such as sucralose (**4a**) and aspartame (**4b**) in water (Fig. 4, E and F, figs. S25 to S27, and scheme S4) (*42*, *43*). The competitive encapsulation experiments revealed the binding preference in the order of **4a** > **4b** >>> **2a** (figs. S28 and S29, and schemes S5 and S6). The binding constants of **1** toward **4a** and **4b** were estimated to be 24,200 and 13,000 M^{-1}, respectively, by ^{1}H NMR studies (fig. S27). The observed order is the same as the degree of their sweetness toward people. Artificial sugar substitutes **4a** and **4b** are approximately 600 and 200 times sweeter than **2a**, respectively (*42*). Because the size and shape of **4a** are comparable to those of **2a**, the lower hydrophilicity of **4a**, which has three hydrophobic chloro groups, as compared with that of **2a** would enhance its affinity toward the hydrophobic cavity of **1**.

DISCUSSION

Here, we described the selective encapsulation of D-sucrose in water from natural disaccharide mixtures within a nonfunctionalized polyaromatic cavity of a coordination-driven molecular capsule. Unlike previous synthetic molecular receptors, which rely on multiple hydrogen bonding, covalent bonding, coordinative, or ion-dipole interaction sites, the present capsule binds D-sucrose with perfect selectivity through a combination of shape-complementary and specific CH-π (polyaromatic ring) interactions. These results expand the versatility and utility of artificial polyaromatic nanospaces for the selective recognition and isolation of complex biomolecules in water.

MATERIALS AND METHODS

Chemicals

Capsule **1** (*35*) and saccharide **3c** (*44*) were synthesized according to previously reported procedures in the literature. Solvents and reagents were purchased from TCI Co. Ltd., Wako Pure Chemical Industries Ltd., Kanto Chemical Co. Inc., Sigma-Aldrich Co., and Cambridge Isotope Laboratories Inc.

General

The NMR spectra were obtained using Bruker AVANCE III 400 (400 MHz) and ASCEND-500 (500 MHz). The ^{1}H NMR and 2D NMR spectra were measured with tetramethylsilane as the internal standard. The ESI-TOF MS data were obtained using Bruker micrOTOF II. The Fourier transform infrared (FT-IR) spectra were recorded using JASCO FT/IR-4200.

Formation of 1⊃2a

Pt capsule **1** (1.5 mg, 0.39 μmol) and D-sucrose (**2a**; 0.7 mg, 2.0 μmol) were added to a glass test tube containing D_2O (0.5 ml). The mixture was stirred for 30 min at 60°C. The formation of 1:1 host-guest complex **1**⊃**2a** was confirmed by NMR and ESI-TOF MS analyses (86% yield based on **1**). Thermodynamic parameters of the encapsulation of **2a** by capsule **1** were estimated by temperature-dependent ^{1}H NMR analysis. The binding constants (K_a = [**1**⊃**2b**]/[**1**]•[**2b**]) were determined on the basis of the integral ratios of the host-guest proton signals (fig. S22 and table S3). The thermodynamic parameters (ΔH and ΔS) were calculated from ΔG values obtained at 298 to 338 K (Fig. 3G, fig. S21, and table S2) (*45*).

^{1}H NMR (500 MHz, D_2O, room temperature): δ −1.14 (t, J = 9.5 Hz, 1H, **2a**), −0.75 (d, J = 9.5 Hz, 1H, **2a**), −0.67 (d, J = 12 Hz, 1H, **2a**), −0.32 (d, J = 12 Hz, 1H, **2a**), 0.04 to 0.09 (m, 2H, **2a**), 0.22 (m, 1H, **2a**), 0.34 to 0.45 (m, 2H, **2a**), 0.62 (t, J = 9.5 Hz, 1H, **2a**), 0.76 (d, J = 14 Hz, 1H, **2a**), 1.29 (m, 2H, **2a**), 2.43 to 2.48 (s, 24H, **1**), 3.07 (m, 16H, **1**), 3.40 (s, 12H, **1**), 3.88 to 4.20 (m, 24H, **1**), 4.47 (m, 4H, **1**), 4.62 (m, 4H, **1**), 6.33 (s, 4H, **1**), 6.45 (br, 8H, **1**), 6.73 (br, 8H, **1**), 7.01 (d, J = 9.0 Hz, 8H, **1**), 7.15 (br, 8H, **1**), 7.53 (dd, J = 9.0, 7.0 Hz, 8H, **1**), 7.71 (d, J = 9.0 Hz, 8H, **1**), 7.77 (br, 8H, **1**), 8.09 to 8.27 (m, 16H, **1**), 8.32 (dd, J = 8.0, 5.5 Hz, 8H, **1**), 8.54 (d, J = 8.0 Hz, 8H, **1**), 9.21 (d, J = 5.5 Hz, 8H, **1**). ^{1}H NMR (500 MHz, D_2O, 60°C): δ −1.12 (t, J = 9.5 Hz, 1H, **2a**), −0.73 (d, J = 9.0 Hz, 1H, **2a**), −0.66 (d, J = 12 Hz, 1H, **2a**), −0.33 (d, J = 12 Hz, 1H, **2a**), 0.02 (d, J = 9.0 Hz, 1H, **2a**), 0.09 (d, J = 12 Hz, 1H, **2a**), 0.19 (m, 1H, **2a**), 0.29 to 0.43 (m, 3H, **2a**), 0.58 (t, J = 9.5 Hz, 1H, **2a**), 0.73 (d, J = 14 Hz, 1H, **2a**), 1.27 (t, J = 9.0 Hz, 1H, **2a**), 1.30 (s, 1H, **2a**), 2.45 to 2.49 (s, 24H, **1**) 3.08 (m, 16H, **1**), 4.57 to 4.58 (m, 8H, **1**), 6.15 to 6.26 (s, 4H, **1**), 6.34 to 6.45 (m, 8H, **1**), 6.56 to 6.66 (br, 8H, **1**), 6.92 (d, J = 8.5 Hz, 8H, **1**), 7.05 to 7.21 (br, 8H, **1**), 7.48 (dd, J = 9.0, 7.0 Hz, 8H, **1**), 7.65 (d, J = 9.0 Hz, 8H, **1**), 7.74 (dd, J = 9.0, 7.0 Hz, 8H, **1**), 7.95 to 8.04 (m, 8H, **1**), 8.30 (dd, J = 9.5, 5.5 Hz, 8H, **1**), 8.45 to 8.52 (m, 8H, **1**), 9.16 to 9.20 (m, 8H, **1**). ^{1}H DOSY NMR (500 MHz, D_2O, 25°C): $D = 1.48 \times 10^{-10}$ m^2 s^{-1}. FT-IR (KBr, cm^{-1}): 2926, 2883, 2828, 1638, 1384, 1357, 1245, 1195, 1105, 1061, 1031, 945, 821, 768, 706, 671, 639, 617. ESI-TOF MS (H_2O, room temperature): m/z 2041.7 [**1**⊃**2a** − 2•NO_3^-]$^{2+}$, 1340.5 [**1**⊃**2a** − 3•NO_3^-]$^{3+}$, 989.9 [**1**⊃**2a** − 4•NO_3^-]$^{4+}$.

Selective encapsulation of 2a by 1 from mixed disaccharides

Pt capsule **1** (1.5 mg, 0.39 μmol), D-sucrose (**2a**; 0.7 mg, 2.0 μmol), and D-trehalose (**2b**; 0.7 mg, 2.0 μmol) were added to a glass test tube containing D_2O (0.5 ml). The mixture was stirred for 30 min at 60°C. The selective formation of 1:1 host-guest complex **1**⊃**2a** was confirmed by ^{1}H NMR analysis. When a grain of KNO_3 was added to the aqueous solution, a yellow precipitate of **1**⊃**2a** was generated. The ^{1}H NMR spectrum of the collected yellow solid (1.3 mg) in D_2O (0.5 ml) revealed the isolation of **1**⊃**2a** in 80% yield. The selective formation of **1**⊃**2a** was also observed from mixtures of **2a**/**2c**, **2a**/**2d**, **2a**/**2e**, and **2a**/**2f** under the same conditions.

Theoretical calculation of host-guest complexes

The universal force field (UFF) model (*46*) was used for intramolecular potential models and nonelectrostatic interactions, unless otherwise specified. The atomic charges of molecular capsule **1** (R = -OCH_3) were determined by the charge equilibration method (*47*) implemented in the FORCITE module at the geometry of the crystal structure, whereas the atomic charges of saccharides [that is, D-sucrose (**2a**), D-trehalose (**2b**), D-lactose (**2c**), and pentamethylated α-D-glucose (**3b**)] were taken from the GLYCAM06j force field (*48*). The geometry optimizations of all the molecules were performed with the FORCITE module of Materials Studio and the Sander module of an Amber14 suite (*49*). The 10-ns-long annealing simulations of the hydroxy groups on the saccharides from 1000 to 10 K were performed to optimize their orientations before the full-geometry optimizations with the Sander module. The final optimized structures of the molecular capsule and the saccharides were obtained by performing the geometry optimizations implemented in the FORCITE program (fig. S19). Relative binding energies were evaluated with gas-phase binding energies and solvation energies of the saccharides in aqueous solutions on the assumption that differences in solvation energies between the host-guest complexes with the different saccharides are negligible. Given that

the capsular hosts isolated the sugars from bulk water environment, and conformations of the host frameworks in contact with the bulk water molecules were not greatly altered upon the encapsulations, the solvation energies of the host-guest complexes with the different saccharides can be expected to be almost identical. First, the gas-phase binding energies were calculated with the UFF model. Then, the solvation free energies, ΔG_{solv}, were calculated by the finite-difference linearized Poisson-Boltzmann method for electrostatic contributions and the solvent-accessible surface area model for nonpolar contributions (*50*), both of which were implemented in the Amber14 suite. We used default values except for a grid spacing of 0.1 Å and the atomic radii of the modified Bondi ones (*51*). The molecular dynamics simulation was performed with the modified pmemd module in the Amber14 suite (*49*), where the intramolecular geometries were fixed at their optimized structures and the capsule and saccharides were treated as a rigid body (*52*). We used the cubic unit cell of the 44.31 Å edge length, which contained capsule **1** (R = -OCH_3), **2a**, and 2723 TIP3P (transferable intermolecular potential with 3 points) waters (fig. S20).

SUPPLEMENTARY MATERIALS

Supplementary material for this article is available at http://advances.sciencemag.org/cgi/content/full/3/8/e1701126/DC1

scheme S1. Host-guest interactions between **1** and **3a**.
scheme S2. Formation of **1**⊃**3b**.
scheme S3. Host-guest interactions between **1** and **2b**.
scheme S4. Formation of **1**⊃**4a**.
scheme S5. Selective encapsulation of **4a** by **1** from a mixture of **2a** and **4a**.
scheme S6. Competitive binding experiment of **4a** and **4b** by **1**.
fig. S1. ^{1}H NMR spectra (500 MHz, D_2O, room temperature) of **1** with various monosaccharides.
fig. S2. ESI-TOF MS spectra (H_2O, room temperature) of **1** with various monosaccharides.
fig. S3. Temperature-dependent ^{1}H NMR spectra (500 MHz, D_2O) of **1**⊃**3b**.
fig. S4. ^{1}H DOSY NMR spectrum (500 MHz, D_2O, 25°C) of **1**⊃**3b**.
fig. S5. 1D NOESY spectrum (500 MHz, D_2O, room temperature, irradiation at 7.96 ppm) of **1**⊃**3b**.
fig. S6. Concentration-dependent ^{1}H NMR spectra (500 MHz, D_2O, room temperature) of **1**⊃**3b**.
fig. S7. ESI-TOF MS spectrum (H_2O, room temperature) of **1**⊃**3b** at 5.0 μM.
fig. S8. ESI-TOF MS spectrum (H_2O, room temperature) of **1**⊃**3b**.
fig. S9. Optimized structure of **1**⊃**3b** (R = -OCH_3).
fig. S10. ^{1}H NMR spectra (500 MHz, D_2O, room temperature) of **1**⊃**2a**.
fig. S11. ^{1}H NMR spectra (500 MHz, D_2O, 60°C) of **1**⊃**2a**.
fig. S12. ^{1}H-^{1}H Correlation spectroscopy (COSY) spectra (500 MHz, D_2O, room temperature) of **1**⊃**2a**.
fig. S13. NOESY spectra (500 MHz, D_2O, room temperature) of **1**⊃**2a**.
fig. S14. Homonuclear Hartmann-Hahn (HOHAHA) spectrum (500 MHz, D_2O, 60°C) of **1**⊃**2a**.
fig. S15. Heteronuclear single quantum coherence (HSQC) NMR spectrum (500 MHz, D_2O, 60°C) of **1**⊃**2a**.
fig. S16. ^{1}H DOSY NMR spectrum (500 MHz, D_2O, room temperature) of **1**⊃**2a**.
fig. S17. ESI-TOF MS spectrum (H_2O, room temperature) of **1**⊃**2a**.
fig. S18. ^{1}H NMR spectra (500 MHz, D_2O, room temperature) of **1** with various disaccharides.
fig. S19. Optimized structure of **1**⊃**2a** (R = -OCH_3).
fig. S20. A snapshot of **1**⊃**2a** (R = -OCH_3) in water from molecular dynamics simulation.
fig. S21. Temperature-dependent ^{1}H NMR spectra (500 MHz, D_2O) of **1**⊃**2a**.
fig. S22. Concentration-dependent ^{1}H NMR spectra (500 MHz, D_2O, 0.155 mM based on **1**, room temperature) of **1**⊃**2a**.
fig. S23. Selective encapsulation of **2a** from a mixture of **2a** and **2b** by **1**.
fig. S24. Selective encapsulation of **2a** from a mixture of **2a** and various disaccharides by **1**.
fig. S25. Encapsulation of **4a** within **1**.
fig. S26. Encapsulation of **4b** within **1**.
fig. S27. Concentration-dependent ^{1}H NMR spectra (500 MHz, D_2O, 0.8 mM based on **1**, room temperature) of **1**⊃**4a** and **1**⊃**4b**.
fig. S28. Competitive binding experiments of **2a** and artificial sugars by **1**.
fig. S29. Competitive binding experiment of **4a** and **4b** by **1**.
table S1. Theoretical binding energies of host-guest complexes (R = -OCH_3).
table S2. Thermodynamic parameters of **1**⊃**2a**.
table S3. Binding constants of **1** toward **2a** in water.

REFERENCES AND NOTES

1. K. E. Avis, V. L. Wu, *Biotechnology and Biopharmaceutical Manufacturing, Processing, and Preservation* (CRC Press, 1996).
2. R. V. Stick, *Carbohydrates: The Sweet Molecules of Life* (Academic Press, 2001).
3. T. K. Lindhorst, *Essentials of Carbohydrate Chemistry and Biochemistry* (John Wiley & Sons, 2007).
4. H.-J. Böhm, G. Schneider, *Protein-Ligand Interactions: From Molecular Recognition to Drug Design* (John Wiley & Sons, 2005).
5. A. B. Hughes, *Amino Acids, Peptides and Proteins in Organic Chemistry, Volume 2, Modified Amino Acids, Organocatalysis and Enzymes* (John Wiley & Sons, 2009).
6. M.-I. Kim, H.-S. Kim, J. Jung, S. Rhee, Crystal structures and mutagenesis of sucrose hydrolase from *Xanthomonas axonopodis* pv. *glycines*: Insight into the exclusively hydrolytic amylosucrase fold. *J. Mol. Biol.* **380**, 636–647 (2008).
7. P. Rios, T. S. Carter, T. J. Mooibroek, M. P. Crump, M. Lisbjerg, M. Pittelkow, N. T. Supekar, G.-J. Boons, A. P. Davis, Synthetic receptors for the high-affinity recognition of O-GlcNAc derivatives. *Angew. Chem. Int. Ed.* **55**, 3387–3392 (2016).
8. Y. Ferrand, M. P. Crump, A. P. Davis, A synthetic lectin analog for biomimetic disaccharide recognition. *Science* **318**, 619–622 (2007).
9. B. Sookcharoenpinyo, E. Klein, Y. Ferrand, D. B. Walker, P. R. Brotherhood, C. Ke, M. P. Crump, A. P. Davis, High-affinity disaccharide binding by tricyclic synthetic lectins. *Angew. Chem. Int. Ed.* **51**, 4586–4590 (2012).
10. M. Rauschenberg, S. Bomke, U. Karst, B. J. Ravoo, Dynamic peptides as biomimetic carbohydrate receptors. *Angew. Chem. Int. Ed.* **49**, 7340–7345 (2010).
11. T. D. James, K. R. A. S. Sandanayake, S. Shinkai, A glucose-selective molecular fluorescence sensor. *Angew. Chem. Int. Ed.* **33**, 2207–2209 (1994).
12. S. Striegler, M. G. Gichinga, Disaccharide recognition by binuclear copper(II) complexes. *Chem. Commun.* 5930–5932 (2008).
13. Y. Jang, R. Natarajan, Y. H. Ko, K. Kim, Cucurbit[7]uril: A high-affinity host for encapsulation of amino saccharides and supramolecular stabilization of their α-anomers in water. *Angew. Chem. Int. Ed.* **53**, 1003–1007 (2014).
14. A. P. Davis, R. S. Wareham, Carbohydrate recognition through noncovalent interactions: A challenge for biomimetic and supramolecular chemistry. *Angew. Chem. Int. Ed.* **38**, 2978–2996 (1999).
15. M. Mazik, Molecular recognition of carbohydrates by acyclic receptors employing noncovalent interactions. *Chem. Soc. Rev.* **38**, 935–956 (2009).
16. D. B. Walker, G. Joshi, A. P. Davis, Progress in biomimetic carbohydrate recognition. *Cell. Mol. Life Sci.* **66**, 3177–3191 (2009).
17. X. Sun, T. D. James, Glucose sensing in supramolecular chemistry. *Chem. Rev.* **115**, 8001–8037 (2015).
18. G. Nelson, M. A. Hoon, J. Chandrashekar, Y. Zhang, N. J. P. Ryba, C. S. Zuker, Mammalian sweet taste receptors. *Cell* **106**, 381–390 (2001).
19. X. Li, L. Staszewski, H. Xu, K. Durick, M. Zoller, E. Adler, Human receptors for sweet and umami taste. *Proc. Natl. Acad. Sci. U.S.A.* **99**, 4692–4696 (2002).
20. J. Chandrashekar, M. A. Hoon, N. J. P. Ryba, C. S. Zuker, The receptors and cells for mammalian taste. *Nature* **444**, 288–294 (2006).
21. M. Fujita, M. Tominaga, A. Hori, B. Therrien, Coordination assemblies from a Pd(II)-cornered square complex. *Acc. Chem. Res.* **38**, 369–378 (2005).
22. M. M. J. Smulders, I. A. Riddell, C. Browne, J. R. Nitschke, Building on architectural principles for three-dimensional metallosupramolecular construction. *Chem. Soc. Rev.* **42**, 1728–1754 (2013).
23. T. R. Cook, P. J. Stang, Recent developments in the preparation and chemistry of metallacycles and metallacages via coordination. *Chem. Rev.* **115**, 7001–7045 (2015).
24. C. J. Brown, F. D. Toste, R. G. Bergman, K. N. Raymond, Supramolecular catalysis in metal–ligand cluster hosts. *Chem. Rev.* **115**, 3012–3035 (2015).
25. W. Wang, Y.-X. Wang, H.-B. Yang, Supramolecular transformations within discrete coordination-driven supramolecular architectures. *Chem. Soc. Rev.* **45**, 2656–2693 (2016).
26. C. He, Z. Lin, Z. He, C. Duan, C. Xu, Z. Wang, C. Yan, Metal-tunable nanocages as artificial chemosensors. *Angew. Chem. Int. Ed.* **47**, 877–881 (2008).
27. Y. Liu, X. Wu, C. He, Y. Jiao, C. Duan, Self-assembly of cerium-based metal–organic tetrahedrons for size-selectively luminescent sensing natural saccharides. *Chem. Commun.* 7554–7556 (2009).
28. T. Andersson, K. Nilsson, M. Sundahl, G. Westman, O. Wennerström, C_{60} embedded in γ-cyclodextrin: A water-soluble fullerene. *Chem. Commun.* 604–606 (1992).
29. Z.-i Yoshida, H. Takekuma, S.-i. Takekuma, Y. Matsubara, Molecular recognition of C_{60} with γ-cyclodextrin. *Angew. Chem. Int. Ed.* **33**, 1597–1599 (1994).
30. C. N. Murthy, K. E. Geckeler, Synthetic approaches for the nanoencapsulation of fullerenes. *Curr. Org. Synth.* **3**, 1–7 (2006).
31. M. Yoshizawa, J. K. Klosterman, Molecular architectures of multi-anthracene assemblies. *Chem. Soc. Rev.* **43**, 1885–1898 (2014).
32. M. Yoshizawa, M. Yamashina, Coordination-driven nanostructures with polyaromatic shells. *Chem. Lett.* **46**, 163–171 (2017).

33. N. Kishi, Z. Li, K. Yoza, M. Akita, M. Yoshizawa, An M_2L_4 molecular capsule with an anthracene shell: Encapsulation of large guests up to 1 nm. *J. Am. Chem. Soc.* **133**, 11438–11441 (2011).
34. N. Kishi, Z. Li, Y. Sei, M. Akita, K. Yoza, J. S. Siegel, M. Yoshizawa, Wide-ranging host capability of a Pd^{II}-linked M_2L_4 molecular capsule with an anthracene shell. *Chem. Eur. J.* **19**, 6313–6320 (2013).
35. M. Yamashina, Y. Sei, M. Akita, M. Yoshizawa, Safe storage of radical initiators within a polyaromatic nanocapsule. *Nat. Commun.* **5**, 4662 (2014).
36. M. Yamashina, M. M. Sartin, Y. Sei, M. Akita, S. Takeuchi, T. Tahara, M. Yoshizawa, Preparation of highly fluorescent host–guest complexes with tunable color upon encapsulation. *J. Am. Chem. Soc.* **137**, 9266–9269 (2015).
37. C. L. D. Gibb, B. C. Gibb, Well-defined, organic nanoenvironments in water: The hydrophobic effect drives a capsular assembly. *J. Am. Chem. Soc.* **126**, 11408–11409 (2004).
38. M. Nishio, Y. Umezawa, K. Honda, S. Tsuboyama, H. Suezawa, CH/π hydrogen bonds in organic and organometallic chemistry. *CrystEngComm* **11**, 1757–1788 (2009).
39. M. Nishio, The CH/π hydrogen bond in chemistry. Conformation, supramolecules, optical resolution and interactions involving carbohydrates. *Phys. Chem. Chem. Phys.* **13**, 13873–13900 (2011).
40. K. Yazaki, Y. Sei, M. Akita, M. Yoshizawa, A polyaromatic molecular tube that binds long hydrocarbons with high selectivity. *Nat. Commun.* **5**, 5179 (2014).
41. M. Yamashina, S. Matsuno, Y. Sei, M. Akita, M. Yoshizawa, Recognition of multiple methyl groups on aromatic rings by a polyaromatic cavity. *Chem. Eur. J.* **22**, 14147–14150 (2016).
42. D. J. Ager, D. P. Pantaleone, S. A. Henderson, A. R. Katritzky, I. Prakash, D. E. Walters, Commercial, synthetic nonnutritive sweeteners. *Angew. Chem. Int. Ed.* **37**, 1802–1817 (1998).
43. K. Masuda, A. Koizumi, K.-i. Nakajima, T. Tanaka, K. Abe, T. Misaka, M. Ishiguro, Characterization of the modes of binding between human sweet taste receptor and low-molecular-weight sweet compounds. *PLOS ONE* **7**, e35380 (2012).
44. H. Wang, L. Sun, S. Glazebnik, K. Zhao, Peralkylation of saccharides under aqueous conditions. *Tetrahedron Lett.* **36**, 2953–2956 (1995).
45. S. Hiraoka, K. Harano, M. Shiro, M. Shionoya, Quantitative dynamic interconversion between Ag^{I}-mediated capsule and cage complexes accompanying guest encapsulation/release. *Angew. Chem. Int. Ed.* **44**, 2727–2731 (2005).
46. A. K. Rappe, C. J. Casewit, K. S. Colwell, W. A. Goddard III, W. M. Skiff, UFF, a full periodic table force field for molecular mechanics and molecular dynamics simulations. *J. Am. Chem. Soc.* **114**, 10024–10035 (1992).
47. A. K. Rappe, W. A. Goddard III, Charge equilibration for molecular dynamics simulations. *J. Phys. Chem.* **95**, 3358–3363 (1991).
48. K. N. Kirschner, A. B. Yongye, S. M. Tschampel, J. González-Outeiriño, C. R. Daniels, B. L. Foley, R. J. Woods, GLYCAM06: A generalizable biomolecular force field. Carbohydrates. *J. Comput. Chem.* **29**, 622–655 (2008).
49. D. A. Case, V. Babin, J. T. Berryman, R. M. Betz, Q. Cai, D. S. Cerutti, T. E. Cheatham III, T. A. Darden, R. E. Duke, H. Gohlke, A. W. Goetz, S. Gusarov, N. Homeyer, P. Janowski, J. Kaus, I. Kolossváry, A. Kovalenko, T. S. Lee, S. LeGrand, T. Luchko, R. Luo, B. Madej, K. M. Merz, F. Paesani, D. R. Roe, A. Roitberg, C. Sagui, R. Salomon-Ferrer, G. Seabra, C. L. Simmerling, W. Smith, J. Swails, R. C. Walker, J. Wang, R. M. Wolf, X. Wu, P. A. Kollman, "AMBER 14" (University of California, San Francisco, 2014).
50. D. Sitkoff, K. A. Sharp, B. Honig, Accurate calculation of hydration free energies using macroscopic solvent models. *J. Phys. Chem.* **98**, 1978–1988 (1994).
51. A. Onufriev, D. Bashford, D. A. Case, Exploring protein native states and large-scale conformational changes with a modified generalized born model. *Proteins* **55**, 383–394 (2004).
52. A. Dullweber, B. Leimkuhler, R. McLachlan, Symplectic splitting methods for rigid body molecular dynamics. *J. Chem. Phys.* **107**, 5840–5851 (1997).

Acknowledgments: M. Yamashina thanks the Japan Society for the Promotion of Science (JSPS) for an Overseas Research Fellowship. **Funding:** This study was supported by the JSPS KAKENHI (grant nos. JP25104011/JP26288033/JP17H05359) and Support for Tokyotech Advanced Researchers (STAR). **Author contributions:** M. Yamashina and M. Yoshizawa designed the work, carried out the research, analyzed the data, and wrote the paper. M.A., T.H., and S.H. were involved in the work discussion. T.H. and S.H. contributed to the theoretical calculations. M. Yoshizawa is the principal investigator. All authors discussed the results and commented on the manuscript. M. Yoshizawa claims responsibility for all figures in the main text and the Supplementary Materials. **Competing interests:** The authors declare that they have no competing interests. **Data and materials availability:** All data needed to evaluate the conclusions in the paper are present in the paper and/or the Supplementary Materials. Additional data related to this paper may be requested from the authors.

Submitted 10 April 2017
Accepted 1 August 2017
Published 25 August 2017
10.1126/sciadv.1701126

Citation: M. Yamashina, M. Akita, T. Hasegawa, S. Hayashi, M. Yoshizawa, A polyaromatic nanocapsule as a sucrose receptor in water. *Sci. Adv.* **3**, e1701126 (2017).

Science Advances

A polyaromatic nanocapsule as a sucrose receptor in water

Masahiro Yamashina, Munetaka Akita, Taisuke Hasegawa, Shigehiko Hayashi and Michito Yoshizawa

Sci Adv **3** (8), e1701126.
DOI: 10.1126/sciadv.1701126